Ligand binding mechanism in steroid receptors; from conserved plasticity to differential evolutionary constraints.

Karl Edman[1, *], Ali Hosseini[2], Magnus K Bjursell[3], Anna Aagaard[1], Lisa Wissler[1], Anders Gunnarsson[1], Tim Kaminski[1], Christian Köhler[4], Stefan Bäckström[1], Tina J Jensen[4], Anders Cavallin[4], Ulla Karlsson[1], Ewa Nilsson[1], Daniel Lecina[2], Ryoji Takahashi[2], Christoph Grebner[5], Stefan Geschwindner[1], Matti Lepistö[4], Anders C Hogner[5, *] and Victor Guallar[2,6, *]

Affiliations and contact information

[1]Discovery Sciences, AstraZeneca, Mölndal, Pepparedsleden 1, 43183, Mölndal, Sweden

[2]Joint BSC-CRG-IRB Research Program in Computational Biology, Barcelona Supercomputing Center, Jordi Girona 29, E-08034 Barcelona, Spain

[3]R&D Information, AstraZeneca, Pepparedsleden 1, 43183, Mölndal, Sweden

[4]RIA, AstraZeneca, Pepparedsleden 1, 43183, Mölndal, Sweden

[5]CVMD, AstraZeneca, Pepparedsleden 1, 43183, Mölndal, Sweden

[6]Institució Catalana de Recerca i Estudis Avançats (ICREA), Passeig Lluís Companys 23, E-08010 Barcelona, Spain

*Corresponding authors:

anders.hogner@astrazeneca.com (A.C.H.), victor.guallar@bsc.es (V.G.), karl.edman@astrazeneca.com (K.E.)

Summary

Steroid receptor drugs have been available for more than half a century, but details of the ligand binding mechanism has remained elusive. We solved X-ray structures of the glucocorticoid and mineralocorticoid receptors to identify a conserved plasticity at helix 6-7 region that extend the ligand binding pocket towards the receptor surface. Since none of the endogenous ligands exploit this region, we hypothesized that it constitutes an integral part of the binding event. Extensive all atom unbiased ligand exit and entrance simulations corroborate a ligand binding pathway that gives the observed structural plasticity a key functional role. Kinetic measurements reveal that the receptor residence time correlate with structural rearrangements observed in both structures and simulations. Ultimately, our findings reveal why nature has conserved the capacity to open up this region and highlight how differences in the details of the ligand entry process result in differential evolutionary constraints across the steroid receptors.

Introduction

Biological functions originate from, and are maintained by, a combination of genomic drift and selection. The traditional method to derive evolutionary relationships is to compare primary sequences, tertiary structures and protein function. However, while changes in the amino acid sequence and placement of key residues provide useful insights into lineage, this only provides the basic framework for mechanistic detail. A more complete functional understanding requires protein plasticity to be considered. Moreover, comparing protein flexibility of related systems adds an important dimension when exploring evolutionary trajectories (Bhabha et al., 2013).

The steroid receptor family consists of five closely related receptors: the mineralocorticoid receptor (MR), the glucocorticoid receptor (GR), the androgen receptor (AR), the progesterone receptor (PR) and the estrogen receptors (ERα and ERβ) (Figure. 1A). They all bind cholesterol derivatives and play a critical role in fundamental biological processes, ranging from pregnancy, early development, to the stress response and electrolyte homeostasis (Evans et al., 1988 and Mangelsdorf et al., 1995). Continual pharmaceutical efforts have resulted in several efficacious drugs across the family (Cole et al., 2006, Gravez et al., 2013, Shelle et al., 2008, Sitruk-Ware et al., 2010 and Alexander et al., 2013). However, target class-related side-effects limit the prescription of these drugs for many indications and the scope for further improvement is considered to be high (Bertocchio et al., 2011). The receptors share a common architecture with three separate domains: the N-terminal domain (NTD), the DNA binding domain (DBD) and the ligand binding domain (LBD). Besides recognizing the ligand pharmacophore, the LBD also contains the activation function-2 (AF-2), which is important for transmitting ligand binding information and partially driving the co-regulator interaction fingerprint (Gronemeyer et al., 2004). In the resting state, the receptors are associated with chaperone proteins in the cytoplasm. Ligand activation leads to a partial release of chaperone proteins, followed almost always by nuclear translocation. In the nucleus, the receptors dimerize and form ligand and context specific protein complexes, resulting in activation and/or repression of gene transcription.

All steroid receptor LBD structures exhibit the typical 3-layered alpha helical fold that fully encloses the various compounds in the ligand binding pocket (Bledsoe et al., 2002, Williams et al., 1998, Fagart et al., 2005 and Matias et al., 2000), Figure 1B.

When overlaying the steroid receptors, the largest structural difference in proximity to the ligand is located in the region where helices 3, 7 and 11 meet (Li et al., 2005). Figure 1C shows a detailed comparison of GR to its paralog MR. An outward tilt of the helix 6–7 (H6-H7) interface in GR results in an expanded ligand binding pocket, and the most potent GR ligands contain large substituents extending in this direction (17α). Despite the smaller pocket in MR, several ligands with bulky 17α substituents on the steroidal D-ring, such as desisobutyrylciclesonide (dibC, the active metabolite of the pro-drug ciclesonide), are more potent in the MR binding assay than the endogenous agonist aldosterone.

Plasticity in the H6-H7 region has been reported for ERα, AR and PR (Andrieu et al., 2015, Nettles et al., 2007 and Kohn et al., 2012) and appears to be a conserved feature across the nuclear receptor superfamily (Soisson et al., 2008 and Hughes et al., 2012). To build a detailed understanding for how the differences in receptor design influence the H6-H7 rearrangments, we determined the X-ray structures of both MR and GR in complex with dexamethasone and dibC (Figure 1D). The structures revealed that when binding a ligand with a large 17α substituent, MR is fully capable of adopting an open structural conformation and that the nature of these rearrangements are clearly distinct from analogous changes in GR. Why has nature preserved the capacity to open up this region across the steroid receptor family, even though it is not exploited by the endogenous ligands? Our hypothesis is that the observed plasticity is an integral part of the ligand entry mechanism.

To test this hypothesis we performed comprehensive all atom unbiased simulations. In these studies, we could link the observed plasticity in the H6-H7 region to the

ligand binding mechanism. While the simulations clearly identified a common binding trajectory for the two receptors, they also highlighted detailed differences in the entry and exit processes. By employing Surface Plasmon Resonance (SPR) and Single Molecule Microscopy (SMM), we could show that these differences correlate with distinct ligand-receptor residence times. Finally, we perform a bioinformatic analyses where we confirm that GR has relaxed evolutionary constraints on the H6-H7 amino acid sequence relative all other steroid receptors. The link to the ligand binding utility provides a functional understanding for these observations.

Results

A conserved plasticity

Dexamethasone was originally developed as a GR specific agonist (Alexander et al., 2013) and was used to determine the first GR LBD structre (Bledsoe et al., 2002). However, dexamethasone was later shown to also be a potent MR ligand in a functional reporter gene assay (Rupprecht et al., 1993). The X-ray structure of MR in complex with dexamethasone (MR:Dexa, Figure 2A) is similar to the corresponding GR:Dexa structure (normalized root mean square deviation (RMSD) of 0.37 Å for 100 Cα atoms). However, examining the region where helices 3, 7 and 11 meet, confirms that the 17α sub-pocket is considerably smaller in the MR structure compared with the GR structure (Figure 1C). This is reflected in the total volume of the MR:Dexa ligand binding pocket, which is approximately 543 $Å^3$ compared with 572 $Å^3$ in the GR:Dexa structure (Figure S1).

It has been proposed that structural differences in the loop between helices 6 and 7 are primarily due to replacement of $Ser843^{MR}$ by $Pro637^{GR}$, which alters the

geometrical constraints of this region and allows GR to adopt a more open conformation (Li et al., 2005). However, despite the limited size of the MR sub-pocket, dibC has higher affinity than aldosterone in the scintillation proximity assay (SPA) using tritiated aldosterone and MR LBD fusion protein (K_i for dibC is 0.18 nM compared to 1.0 nM for aldosterone, Figure S2). To study the structural flexibility associated with large 17α substituents, we determined the complex structures of MR:dibC and GR:dibC.

The structure of MR:dibC superimposes well on the MR:Dexa structure (normalized RMSD of 0.28 Å for 100 Cα atoms). dibC is placed in a nearly identical position as dexamethasone in the binding pocket, with all polar interactions conserved (Figure 2B). In addition, the AF-2 surface remains virtually unchanged, with key interactions to the NCOA1 peptide intact. However, while these two receptor conformations are closely related, dibC induces a large rearrangement of the H6-H7 loop region, essentially extending the ligand binding pocket towards the receptor surface (Figure 3A). Specifically, side chains of $Ser843^{MR}$, $Met845^{MR}$ and $Cys849^{MR}$ in the MR:Dexa complex occupy the same volume as the cyclohexyl motif of dibC, forcing the receptor to adopt a new conformation (Figure 3B). This leads to a repositioning of helix 6 and an extension of helix 7. While $Ser843^{MR}$ was previously buried within the protein and engaged in a hydrogen bond to the backbone nitrogen of $Met845^{MR}$, it is now exposed to the solvent, forming the new start of helix 7 (Figure 3A). Recent data suggests that phosphorylation of this residue affects both ligand binding and receptor translocation into the nucleus (Shibata et al., 2013). The structural changes observed here explain how the receptor may use the local plasticity to make $Ser843^{MR}$ available for modification.

The size of the 17α pocket in the MR:dibC complex increases significantly (total ligand binding pocket volume 714 $Å^3$, Figure S1) and the superposition on the GR:Dexa structure shows that this region now adopts a more closely related structural state (Figure 3C). Finally, while GR in complex with dibC (Figure 3D) expands the 17α pocket (total ligand binding pocket volume 661 $Å^3$, Figure S1) relative to the GR:Dexa structure, it does not alter any of the secondary structural elements. Instead, the H6-H7 region appears to be shifted in a rigid way in response to cyclohexyl of dibC. While plasticity in the H6-H7 region seems to be conserved across these two receptors, the details of the ligand driven rearrangements are different.

To quantify the flexibility in the H6-H7 region across the steroid receptor family, we performed principal component analysis (PCA) for all X-ray structures from the protein data bank (PDB) for each receptor. This allows visualization of the variance between structures as a set of normal modes. While the description of this variance will be highly dependent on what regions of the binding pocket are exploited by the various ligands, the mode describing H6-H7 motion is one of the strong features (Figure S3). However, for MR the H6-H7 motion is only prominent if we include the MR:dibC structure from this work, emphasizing that the MR:dibC structure describes a novel structural conformation.

Modeling non biased entry and exit pathways

Spontaneous ligand binding events have been investigated using molecular dynamics in both exposed (Buch et al., 2011), and partially exposed binding sites (Dror et al., 2011). However, nuclear receptors have fully occluded binding pockets that likely require significant rearrangements for ligand entry. Therefore we decided

to use PELE (Borrelli et al., 2005), which is an alternative approach that use Monte Carlo algorithms with structural prediction for efficient sampling of the protein-ligand energy landscape. For ligand escape simulations the MR and GR X-ray complex structures were used as the starting position. For ligand binding studies, the ligand was randomly placed in the bulk solvent and allowed to freely migrate. All simulations were completed in the presence and absence of a co-factor peptide at the AF-2 site (NCOA1 residues 1430-1441 for MR and NCOA2 residues 741-753 for GR). In addition, both the wild-type protein sequences and the specific mutants present in the X-ray structures were used.

Ligand dissociation

For all permutations of both MR and GR, we performed three separate exit simulations, observing only one exit trajectory perforating the surface where helices 3, 7 and 11 meet. Figure 4A illustrates the MR:Dexa exit pathway simulation with the array of dexamethasone positions superimposed on the initial MR structure. Notably, ligand motion is coupled with significant rearrangement of the protein backbone along the migration pathway. In particular, the loop connecting helices 6 and 7 is shifted outwards to accommodate ligand release (Figure 4B). Interestingly, the simulated protein movements mimic the differences between the MR:Dexa and MR:dibC structures shown in light and dark blue, respectively. Root mean square fluctuations (RMSF) along the exit trajectory (Figure 4C) clearly show that the movements of the H6-H7 region are considerable larger than for the rest of the protein.

Figure 5 shows the corresponding simulation for GR:Dexa (equivalent simulations for MR:dibC and GR:dibC resulted in the same exit trajectory). Based on the complete set of ligand dissociation simulations it is apparent that both MR and GR have the same ligand unbinding pathway. In addition, while ligand exit is associated with similar protein motions, the fluctuations in the H6-H7 region are significantly larger for MR than for GR (Figure 5c). This is in agreement with the idea that GR would require smaller rearrangements, because the receptor is more open to begin with.

Ligand association

To investigate ligand entry we randomly placed dexamethasone in the bulk solvent and released it to freely probe the protein surface. For each receptor we performed five runs with 64 independent trajectories over 48 hours. Each run yielded 1-2 trajectories where the ligand entered the binding pocket. In all runs the ligand is free to move without any predefined search direction.

Figure 6A shows the evolution of the ligand heavy atom RMSD to the crystallographic complex for one of the MR:Dexa runs. It is clear that most of the trajectories explore the receptor surface with some excursions into the bulk solvent. However, the blue and red trajectories enter the ligand binding pocket at steps ~50 and ~210, respectively. While the entry along the blue trajectory is relatively fast, the red demonstrates the unbiased nature of the simulation, probing a large portion of the receptor surface before finding the entrance pathway. Figure 6B shows representative ligand centers of mass along these trajectories superimposed on the initial protein structure with the entry to the binding pocket denoted by a surface representation. The corresponding ligand entry simulation for GR is shown in Figure S4. In keeping with the ligand escape simulations for all runs in both systems,

trajectories entering the ligand binding pocket pierce the protein surface at the H3-H7-H11 junction. The MR:Dexa binding event is demonstrated in greater detail in the Supplementary movie.

While the mutants used in the X-ray structures did not influence the simulations significantly, removal of co-factor peptide at the AF-2 resulted in larger fluctuations in both the helix 12 and the H3-H7-H11 junction along the exit and entrance trajectories. However, the ligand entry pathway remained unchanged. The presence of co-regulator peptide has been shown to affect the ligand binding kinetics (Pfaff et al., 2010).

Active site ligand refinement and binding free energy

Once the entrance path to the MR binding pocket had been located, we refined the free search with local enhanced sampling to obtain a precise pose for the best binder. This procedure does not add any bias in the ligand search direction, but it limits the sampling to the region around the entrance point (typically 10-15 Å). Figure 7A shows the interaction energy profile plotted against the ligand heavy atom RMSD to the crystallographic complex for the MR:Dexa refining process (400 trajectories). The lowest binding energies are derived from poses located within 0.75 Å RMSD of the X-ray ligand conformation. The sampling places dexamethasone in the accurate orientation with the A-ring 3-keto moiety pointing toward the $Arg817^{MR}$-$Gln776^{MR}$ pair from helices 5 and 3, and the D-ring hydroxyacetyl approaching the $Asn770^{MR}$ on the N-terminal half of helix3 (Figure 7B). Studying the protein-ligand interaction energy plot in more detail (Figure 7A), it is interesting to note that the surface exploration exhibit a local minima near RMSD of 12 Å. In the crystal structure of GR:Dexa and GR:dibC, this site is occupied by a steroid-like CHAPS molecule that is part of the

protein formulation (Figure S5). In addition, for MR a non-steroidal antagonist has been observed at this position (Hasui et al., 2011). As such, the region may correspond to a peripheral binding site at the H3-H7-H11 junction and the energy barrier located at the 11-12 Å segment in Figure 7A reflect the energy cost associated with the surface crossing event through the entry channel.

The fast performance of PELE, together with the local restriction in the refinement exploration, facilitates running hundreds of trajectories. Based upon Markov State Model (MSM) analysis (Takahashi et al., 2014), we used this data to calculate the binding free energies for MR:Dexa and MR:dibC. While absolute values might be slightly shifted due to the absence of an exhaustive surface/bulk exploration, relative values should be in reasonable agreement, because both ligands share entry point and binding site. Figure 7C shows a 2D projection of the potential mean field (PMF) obtained for MR:Dexa along the 400 refinement trajectories. The red area corresponds to the bulk exploration whereas the global minimum, shown in blue, corresponds to ligand positions matching the experimental structure (Figures 7A and B). Integration of the PMF volume at the active site, where we observe a smooth function (as opposed to the bulk solvent or entrance pathway) converges to a binding free energy of -7.5 kcal/mol for dexamethasone and -9.3 kcal/mol for dibC. The difference in binding free energy of 1.8 kcal/mol is in quantitative agreement with the experimental difference of 2.09 kcal/mol (derived from the Ki values of 6.3 nM for dexamethasone and 0.18 nM for dibC).

Residence time measurements

The ligand entry and exit mechanism establishes a functional role for helices 6 and 7 as a gatekeeper. In addition, the simulations revealed that the structural

rearrangements required for ligand entry and exit are significantly different for GR and MR. As a consequence, the ligand binding kinetics should differ for the two receptors. Using both Surface Plasmon Resonance (SPR) and Single Molecule Microscopy (SMM) (Gunnarsson et al., 2015), we measured the residence time of both dexamethasone and dibC by monitoring the time-resolved change in receptor binding to a surface-immobilized co-regulator peptide upon addition of >10-fold concentration excess of a reference compound (Figure S6). The data from all experiments is summarized in Table 2. In all instances, k_{off} is larger for GR than for MR, hence the residence time is longer in MR. This is in agreement with the observations that MR requires a larger rearrangement of the H6-H7 region compared to GR (Figure 4 and Figure 5). In addition, dexamethasone has a larger k_{off} than dibC, reflecting the fact that dibC is a bulkier ligand. Finally, while the different measurement methods result in the same pattern for both GR and MR and dexamethasone and dibC, providing confidence to the analysis, the systematically larger off-rates using SMM likely reflect the temperature difference at which the experiments were conducted (20 °C for SMM and 10 °C for SPR).

Differential selection pressure

Studies on the evolution of GR from the ancestral corticoid receptor revealed that GR has accumulated a number of mutations on and in the proximity of helix 7 that prevents reversal of evolution (Bridgham et al., 2009). As our findings suggest that there is an intimate link to the ligand binding function we decided to investigate the evolutionary consequences across the whole steroid receptor family. To explore this, sequence clusters for each receptor were downloaded from OrthoDB (Waterhouse et al., 2013). The sequences for each receptor were aligned using ClustalX version 2.0

(Larkin et al., 2007) and the pairwise species overlap with GR was selected for each receptor. Each residue position was then assigned a variability score based on the number of different amino acids at that position across the various species. All receptor sequences were overlaid on the GR sequence using X-ray structures to define the equivalent positions. Finally, we plotted the variability score against the amino acid sequence for all receptor pairs (Figure 8). The data confirms that important structural elements of the receptors are relatively conserved. For example, the variability score for the AF-2 surface (the N-terminal end of H12, H4 and the C-terminal end of H3), which is directly involved in the protein-protein interaction transmitting the ligand activation signal, is consistently low for all receptors. However, H6-H7 exhibits a greater variability score in GR relative to all other receptors. Interestingly, GR also has a segment of higher variability near the C-terminal end of H11. This region sits directly across from the N-terminal end of H7 (Figure 1C) and it is conceivable that amino acid sequences of these regions may well co-vary with each other. Figure S7A shows the variability score for the individual amino acids in the H6-H7 region for the full set of GR species. It is clear that the high variability score of the region resides in discrete positions (primarily in residues 631, 632, 635, 638 and 640). These residues are all located on the outside of the receptor in both the GR:Dexa and GR:dibC structures (Figure S7B).

Discussion

The fundamental role and mechanism of action of steroid receptors have been studied extensively, yet details of the ligand binding mechanisms have remained unclear. By comparing the structures of MR and GR in complex with dexamethasone and dibC, we confirmed the intrinsic capacity to open up the H6-H7 region. While the

GR:Dexa structure adopts an open conformation compared with the MR:Dexa complex, the MR:dibC structure is able to extend the ligand binding pocket significantly and adopt a structural state akin to the GR:Dexa arrangement. Studies of ancestral corticoid receptor (AncCR), the common predecessor of MR and GR, revealed that the Ser106^{AncCR} (corresponding to Ser843^{MR}) to Pro637^{GR} switch was a permissive mutation that facilitated a subsequent Leu111^{AncCR} (corresponding to Leu848^{MR}) to Gln642^{GR} mutation (Bridgham et al., 2006). This is an example of conformational epistasis and has played an important role for the evolution of the GR hormone selectivity (Ortlund et al., 2007). We show that GR and MR demonstrate a similar capacity to form an open conformation, and it is likely that the AncCR also exhibited the same flexibility. Hence, as GR evolved from AncCR, the Ser106^{AncCR} to Pro637^{GR} mutation would primarily serve to select a subset of pre-existing structural states, rather than creating a completely new arrangement. The importance of conformational selection over induced fit has provided mechanistic insights for several biological systems (Changeux et al., 2013), it is plausible that evolution through mutation often operates in an analogous way.

Extensive ligand binding simulations revealed that the entry and exit trajectories all pass through the H3-H7-H11 junction. As the ligand cross the receptor surface, the outward bending motion of the H6-H7 region is qualitatively similar to the observed perturbations caused by the large 17-α cyclohexyl substituent in the dibC complex structures, linking the observed H6-H7 plasticity to the ligand binding mechanism. Interestingly, H7 has also been shown to be important for dimerisation of several nuclear receptors (Osz et al., 2012). This suggests that the two functions could be linked for these receptors, but the strength of that relationship remains to be

determined. The results from the ligand binding simulations indicate that large-amplitude protein motions of helix 12, as suggested by apo and holo crystallographic nuclear hormone receptors (Moras et al., 1998, Yen et al., 2001 and Brzozowski et al., 1997), are not required for ligand entry. Instead, the conformation of the LBD is likely to resemble the ligand bound agonistic conformations of the receptors during the ligand entry step (Capelli et al., 2013 and Batista et al., 2013). We show that small scale vibrations combined with a structural rearrangement of H6-H7 region are enough to identify an energetically favorable pathway to allow the ligands to diffuse into the binding pocket. In contrast to other modeling studies using biased protocols, we do not observe multiple ligand entry or exit pathways (Capelli et al., 2013, Sonoda et al., 2008 and Aci-Sèche et al., 2011). Finally, careful analysis of the binding energies along the entry trajectory revealed a potential peripheral binding site. While it requires further characterization, the function of such a site on the surface of the receptor could serve to capture the ligands and increase the chances for productive binding events.

It is firmly established that steroid receptors depend on a number of chaperone and co-chaperone proteins for correct folding capable of high-affinity hormone binding (Grad et al., 2007). Although the ligand entry function is likely to have evolved before the synergies with chaperone proteins, these proteins will nevertheless limit the access to the receptors and thereby form boundary conditions for any ligand entry hypothesis. Mutation and peptide competition studies suggest that Hsp90 is interacting at the AF-2 surface (Ricketson et al., 2007 and Fang et al., 2006). In addition, co-chaperones have been mapped to interact with regions surrounding the C-terminal end of H1 and the N-terminal end of H3 (Caamaño et al., 1998), and with

the loop that connects them (Cluning et al., 2013). Neither of these areas overlap with the entry site proposed here. However, previous studies have shown that the chaperone complex promote the ligand binding process (Grad et al., 2007). Interestingly, the simulations where we removed the co-regulator peptides resulted in greater fluctuations in both the H3-H7-H11 junction and H12. These results suggest that the presence of chaperone proteins at remote sites can allosterically influence the ligand entry process proposed here.

While the dibC complex structures show that both corticoid receptors can adopt an open conformation, they also highlight that the plasticity in the H6-H7 region is different. For MR, the challenge from a large 17α substituent results in a complete rearrangement of the H6-H7 structure. In contrast, GR responds with a rigid shift of the region. A closer inspection of the simulations revealed ensuing differences as MR require larger rearrangements in the gatekeeper residues for productive ligand binding and unbinding. This is in agreement with the kinetic measurements revealing that both dexamethasone and dibC exhibit longer receptor residence times in MR than GR. However, these observations do not necessarily result in differences in ligand affinity *per se* as both ligand entry and exit will be governed by the same plasticity, potentially affecting on and off rates equally. Nevertheless, it is important to note that ligand binding and unbinding are asymmetric events. While ligand binding occurs with the receptor in the chaperone complex in the cytoplasm, unbinding will likely occur in the different protein complex. As such, it is tempting to speculate that the relative stabilization of the open versus the closed conformation may differ for the two states. This could increase the apparent ligand affinity and potentially add

another layer of differentiation. To resolve this, detailed structural information on the relevant protein complexes would be required.

The distinct receptor blueprints also appear to have evolutionary consequences. By comparing the amino acid sequence for different species across all steroid receptors, we found that GR exhibits a higher mutational frequency in the H6-H7 region. We propose that as GR evolved a cortisol selectivity profile, the change in the dynamic profile of the H6-H7 region, through the $Ser106^{AncCR}$ to $Pro637^{GR}$ mutation, altered the boundary conditions for the ligand entry mechanism. While for MR, residues need to be compatible with two distinct structural states during ligand entry, for GR, the equivalent residues will be exposed to the solvent throughout the process. As a result the selection pressure was relaxed for specific positions in this region for GR, which explains why subsequent mutations could build.

The tremendous growth in the number of available X-ray structures from increasingly more advanced protein classes and complexes provides a plethora of snapshots of molecular mechanism in action. However, to bridge the gap to detailed mechanistic insights and to establish evolutionary relationships, orthogonal data from biochemical experiments and *in silico* modeling are required. By combining information from several X-ray structures, extensive simulations, kinetic measurements and bioinformatic analyses, we have uncovered the ligand binding mechanism into the occluded binding pocket of steroid hormone receptors. Ligand binding to the steroid receptors marks the first step in a chain of events that in the end triggers both broad genomic and non-genomic mechanisms. Understanding the details of ligand

association and dissociation may facilitate the rational design of molecules that exploit the plasticity of the entry and exit processes to a greater extent. This could yield ligands with different modes of action, such as antagonists that block nuclear translocation or agonists with extended receptor occupancy and a prolonged pharmacological response.

Experimental Procedures

Protein expression, purification, crystallization, structure determination and analyses

The detailed protocols are described in the supplementary methods section. For structure, the following protein constructs were used: GR:Dexa, GR-LBD (amino acids 500-777) N517D, F602S, C638D; GR:dibC, GR-LBD (amino acids 500-777) N517D, V571M F602S, C638D; MR:Dexa, MR-LBD (amino acids 735-984) C808S, C910S; MR:dibC, MR-LBD (amino acids 735-984) C808S, S810L C910S. For the kinetic measurements, the following constructs were used: GR, GR-LBD (NR3C1; amino acids 529-777); MR, MR-LBD (amino acids 712-984) C808S.

Mineralocorticoid receptor ligand competition binding assay

A Scintillation proximity (SPA) based radioligand binding assay was used to measure the ligand displacement of aldosterone to human MR-LDB. Detailed protocol is presented in the supplementary experimental procedueres.

PELE simulations

Systems setup

Initial coordinates for GR and MR were obtained from the crystals presented here. Three different receptor models were prepared: 1) the crystallographic structures, 2) the wild type receptors generated by reverting the crystallographic mutations with the Schrödinger package (Schrödinger 2013) , and 3) the wild type receptors in absence of the peptide cofactor. All structures were preprocessed with the protein preparation wizard (Madhavi Sastry et al., 2013) available in the Schrödinger package adding hydrogen atoms and optimizing the hydrogen bond network, followed by a final visual inspection.

PELE sampling

PELE combines a Monte Carlo approach with protein structure prediction methods allowing exploration of long-timescale atomic biophysical processes (Borrelli et al., 2005; Cossins et al., 2012). Three main steps define the algorithm: 1) protein backbone and ligand perturbation, 2) specific side-chain sampling and 3) global minimization (for more details see, for example, Kotev et al., 2015). The program uses an OPLS (Optimized Potentials for Liquid Simulations) all-atom force field with an implicit surface-generalized Born (SGB) continuum solvent model.

Ligand exit simulations

From the crystallographic prepared models, the exit protocol included random ligand's translations of 0.8 Å and rotation of 0.2 radians. The backbone perturbation included the lowest 6 ANM modes with maximum displacements of each alpha carbon up to 1 Å. A spawning criteria of 4 Å was used: any ligand whose center of mass is 4 Å behind the structure with the center of mass farthest coordinates (with respect to the initial position), in any direction, will abandon its position and continue the execution with the coordinates from the leading (farthest) one. Thus, all processors search collectively, with no bias in direction, for an effective escape path. Simulations were finished after the ligand's solvent accessible area (SASA) was larger than 0.5, with typical simulations times of 10-20 CPU hours.

Ligand entrance simulations

Starting from 20 conformations where the ligand is randomly distributed over the protein surface., free search simulations were performed with runs of 64 independent simulations (no spawning criteria was used) for 48 CPU hours. Ligand perturbation included equally probable translations of 3.0 Å / 1.0 Å and rotation of 0.25/0.05 radians.. Ligands displacement direction was randomly updated every 6 steps, thus ensuring that trajectories explore the entire surface. Furthermore, keeping the perturbation direction for 6 steps is necessary to observe entrance events in difficult cases.

Residence time determination

Residence time measurements of GR/MR:dexamethasone and dibC was determined using single molecule microscopy (SMM) and SPR (Biacore). In brief, GR/MR was pre-equilibrated with dexamethasone/dibC. Directly after addition of

budesonide/aldosterone, the rate of receptor binding to the surface-immobilized cofactor peptide, caused by the ligand-induced change in affinity, was monitored continuously over ~15 minutes with SMM or by consecutive injection cycles (typically 6) in SPR. See supporting information for details on surface preparation and experimental procedure. The dissociation rate is was determined by exponential fits to the change in binding rate as a function of time.

Sequence homology analysis

Sequence clusters for each receptor were downloaded from the OrthoDB database (Waterhouse et al., 2013) by searching for the human ENS gene ID and selecting the vertebrate subset. For each receptor, sequences with a length two standard deviations below average length or that contained more than 100 'X' (unknown amino acids) were removed. The sequences for each receptor were aligned using ClustalX version 2.0 (Larkin et al., 2007), then further filtered to only keep sequences with an intact H6-H7 region (max 1 indel or 'X' and >= 50% identity to the human H6-H7 region; sequences with large indels in H6-H7 were removed followed by realignment and refiltering to correct for alignment errors around indels). The filtered sets were scored using custom perl scripts; for each position in the alignment, a variability score was calculated by counting the number of different types of amino acids (i.e. if a position contained 5F, 3Y and 9L, then the score is 3). In order to remove bias stemming from the inclusion of sequences from different species across the various receptors, subsets were generated where the same species were included for pairs of GR with either of [MR, PR, AR, ERα and ERβ]. The paired subsets were realigned for each receptor and the resulting alignments were analyzed and scored as previously described. Finally, the scores were normalized (variability score - average

variability score for LBD) and smoothed using a sliding window of 5 amino acids and plotted against the GR protein sequence.

Phylogenetic analysis of the human LBD region

Human sequences for the studied nuclear receptors (AR, ERα, ERβ, GR, MR and PR) were extracted from the aforementioned dataset. Sequences were trimmed so that only the LBD region remained, aligned using ClustalX and then manually edited based on the structure (minor adjustments). The tree was calculated using ClustalX (bootstrap 1,000 iterations) and visualized using NJplot version 2.3 (Perrière et al., 1996)

Author Contributions

K.E., A.C.H., M.L. and V.G. designed the research. U.K. performed binding experiments. S.B., C.K., T.J.J., A.C. and E.N. expressed and purified protein. A.A. and L.W. crystallized the proteins. K.E. performed the structural determination and analyzed the data. C.G. performed the PCA analysis. A.H. performed the exit and entry simulations. D.L. and R.T. performed MSM analysis. A.G.,T.K and S.G. performed the kinetic experiments. M.K.B. carried out the bioinformatic analysis.

Acknowledgments

This study was supported by The European Research Council (2009-Adg25027-PELE) to V.G and by the SEV-2011-00067 grant of the Severo Ochoa Program. We would like to acknowledge our AstraZeneca colleagues J. Hartleib, R.Unwin and R.Knöll for helpful discussions. We also thank N. Blomberg (ELIXIR) and R. Neutze (University of Gothenburg) for careful reading of the manuscript.

REFERENCES

Aci-Sèche, S., Genest, M., and Garnier, N. (2011). Ligand entry pathways in the ligand binding domain of PPARγ receptor. FEBS Lett. *585*, 2599–2603.

Alexander, S.P.H., Benson, H.E., Faccenda, E., Pawson, A.J., Sharman, J.L., Spedding, M., Peters, J.A., Harmar, A.J. and CGTP Collaborators. (2013). The concise guide to pharmacology 2013/14: Nuclear hormone receptors. Br. J. Pharmacol. *170*, 1652–1675.

Andrieu, T., Mani, O., Goepfert, C., Bertolini, R., Guettinger, A., Setoud, R., Uh, K.Y., Baker, M.E., Frey, F.J., and Frey, B.M. (2015). Detection and functional portrayal of a novel class of dihydrotestosterone derived selective progesterone receptor modulators (SPRM). J. Steroid Biochem. Mol. Biol. *147*, 111–123.

Batista, M.R., and Martínez, L. (2013). Dynamics of nuclear receptor helix-12 switch of transcription activation by modeling time-resolved fluorescence anisotropy decays. Biophys. J. *105*, 1670–1680.

Bertocchio, J., Warnock, D.G., and Jaisser, F. (2011). Mineralocorticoid receptor activation and blockade: an emerging paradigm in chronic kidney disease. Kidney Int. *10*, 1051–1060.

Bhabha, G., Ekiert, D.C., Jennewein, M., Zmasek, C.M., Tuttle, L.M., Kroon, G., Dyson, H.J., Godzik, A., Wilson, I.A., and Wright, P.E. (2013). Divergent evolution of protein conformational dynamics in dihydrofolate reductase. Nat. Struct. Mol. Biol. *11*, 1243–1249.

Bledsoe, R.K., Montana, V.G., Stanley, T.B., Delves, C.J., Apolito, C.J., McKee, D.D., Consler, T.G., Parks, D.J., Stewart, E.L., Willson, T.M., et al. (2002). Crystal structure of the glucocorticoid receptor ligand binding domain reveals a novel mode of receptor dimerization and coactivator recognition. Cell *110*, 93–105.

Borrelli, K.W., Vitalis, A., Alcantara, R., and Guallar, V. (2005). Protein energy landscape exploration. A novel Monte Carlo technique. J. Chem. Theory Comput. *6*, 1304–1311.

Bridgham, J.T., Carroll, S.M., and Thornton, J.W. (2006). Evolution of hormone-receptor complexity by molecular exploitation. Science *312*, 97–101.

Bridgham, J.T., Ortlund, E.A., and Thornton, J.W. (2009). An epistatic ratchet constrains the direction of glucocorticoid receptor evolution. Nature *461*, 515–520.

Brzozowski, A.M., Pike, A.C., Dauter, Z., Hubbard, R.E., Bonn, T., Engström, O., Ohman, L., Greene, G.L., Gustafsson, J.A., and Carlquist, M. (1997). Molecular basis of agonism and antagonism in the oestrogen receptor. Nature *389*, 753–758.

Buch, I., Giorgino, T., and De Fabritiis, G. (2011). Complete reconstruction of an enzyme-inhibitor binding process by molecular dynamics simulations. Proc. Natl. Acad. Sci. USA *108*, 10184–10189.

Caamaño, C.A., Morano, M.I., Dalman, F.C., Pratt, W.B., and Akil, H. (1998). A conserved proline in the hsp90 binding region of the glucocorticoid receptor is required for hsp90 heterocomplex stabilization and receptor signaling. J. Biol. Chem. *273*, 20473–20480.

Capelli, A.M., Bruno, A., Guadix, A.E., and Costantino, G. (2013). Unbinding pathways from the glucocorticoid receptor shed light on the reduced sensitivity of glucocorticoid ligands to a naturally occurring, clinically relevant mutant receptor. J. Med. Chem. *56*, 7003–7014.

602 Changeux, J.P. (2013). 50 years of allosteric interactions: the twists and turns of the
603 models. Nat. Rev. Mol. Cell Biol. *14*, 819–829.

604

605 Cluning, C., Ward, B.K., Rea, S.L., Arulpragasam, A., Fuller, P.J., and Ratajczak, T.
606 (2013). The helix 1-3 loop in the glucocorticoid receptor LBD is a regulatory element
607 for FKBP cochaperones. Mol. Endocrinol. *27*, 1020–1035.

608

609 Cole, T.J. (2006). Glucocorticoid action and the development of selective
610 glucocorticoid receptor ligands. Biotechnol. Annu. Rev. *12*, 269–300.

611

612 Cossins, P.B., Hosseini, A., and Guallar, V. (2012). Exploration of protein
613 conformational change with PELE and meta-dynamics. J. Chem. Theory Comput. *8*,
614 959–965.

615

616 Dror, R.O., Pan, A.C., Arlow, D.H., Borhani, D.W., Maragakis, P., Shan, Y.B., Xu,
617 H.F., and Shaw, D.E. (2011). Pathway and mechanism of drug binding to G-protein-
618 coupled receptors. Proc. Natl Acad. Sci. USA *108*, 13118–13123.

619

620 Evans, R.M. (1988). The steroid and thyroid hormone receptor superfamily. Science
621 *240*, 889–895.

622

623 Fagart, J., Huyet, J., Pinon, G.M., Rochel, M., Mayer, C., and Rafestin-Oblin, M.E.
624 (2005). Crystal structure of a mutant mineralocorticoid receptor responsible for
625 hypertension. Nat. Struct. Mol. Biol. *12*, 554–555.

626

627 Fang, L., Ricketson, D., Getubig, L., and Darimont, B. (2006). Unliganded and
628 hormone-bound glucocorticoid receptors interact with distinct hydrophobic sites in the
629 Hsp90 C-terminal domain. Proc. Natl. Acad. Sci. USA *103*, 18487–18492.

630

631 Grad, I., and Picard, D. (2007). The glucocorticoid responses are shaped by
632 molecular chaperones. Mol. Cell Endocrinol. *275*, 2–12.

633

634 Gravez, B., Tarjus, A., and Jaisser, F. (2013). Mineralocorticoid receptor and cardiac
635 arrhythmia. Clin. Exp. Pharmacol. Physiol. *40*, 910–915.

636

637 Gronemeyer, H., Gustafsson, J.A., and Laudet, V. (2004). Principles for modulation
638 of the nuclear receptor superfamily. Nat. Rev. Drug Discov. *3*, 950–964.

639

640 Gunnarsson, A., Snijder, A., Hicks, J., Gunnarsson, J., Höök, F., and Geschwindner,
641 S. (2015). Drug Discovery at the Single Molecule Level: Inhibition-in-Solution Assay
642 of Membrane-Reconstituted β-Secretase Using Single-Molecule Imaging. Anal.
643 Chem. *87*, 4100–4103.

Hasui, T., Matsunaga, N., Ora, T., Ohyabu, N., Nishigaki, N., Imura, Y., Igata, Y., Matsui, H., Motoyaji, T., Tanaka, T., et al. (2011). Identification of benzoxazin-3-one derivatives as novel, potent, and selective nonsteroidal mineralocorticoid receptor antagonists. J. Med. Chem. *54*, 8616–8631.

Hughes, T.S., Chalmers, M.J., Novick, S., Kuruvilla, D.S., Chang, M.R., Kamenecak, T.M., Rance, M., Johnson, B.A., Burris, T.P., Griffin, P.R. et al. (2012). Ligand and receptor dynamics contribute to the mechanism of graded PPARg agonism. Structure *20*, 139–150.

Jensen, Ø.M., Jogini, V., Borhani, D.W., Leffler, A.E., Dror, R.O., and Shaw, D.E. (2012). Mechanism of voltage gating in potassium channels. Science *336*, 229–233.

Kohn, J.A., Deshpande, K., and Ortlund, E.A. (2012). Deciphering modern glucocorticoid cross-pharmacology using ancestral corticosteroid receptors. J. Biol. Chem. *287*, 16267–16275.

Kotev, M., Lecina, D., Tarragó, T., Giralt, E., and Guallar, V. (2015). Unveiling prolyl oligopeptidase ligand migration by comprehensive computational techniques. Biophys. J. *108*, 116–125.

Larkin, M.A., Blackshields, G., Brown, N.P., Chenna, R., McGettigan, P.A., McWilliam, H., Valentin, F., Wallace, I.M., Wilm, A., Lopez, R., et al. (2007). Clustal W and Clustal X version 2.0. Bioinformatics, *23*, 2947–2948.

Li, Y., Suino, K., Daugherty, J., and Xu, H.E. (2005). Structural and biochemical mechanisms for the specificity of hormone binding and coactivator assembly by mineralocorticoid receptor. Mol. Cell *19*, 367–380.

Madhavi Sastry, G., Adzhigirey, M., Day, T., Annabhimoju, R., and Sherman, W. (2013). Protein and ligand preparation: parameters, protocols, and influence on virtual screening enrichments. J. Comput. Aided Mol. Des. *27*, 221–234.

Mangelsdorf, D.J., Thummel, C., Beato, M., Herrlich, P., Schütz, G., Umesono, K., Blumberg, B., Kastner, P., Mark, M., Chambon, P., and Evans, R.M. (1995). The nuclear receptor superfamily: the second decade. Cell *83*, 835–839.

Matias, P.M., Donner, P., Coelho, R., Thomaz, M., Peixoto, C., Macedo, S., Otto, N., Joschko, S., Scholz, P., Wegg, A., et al. (2000). Structural evidence for ligand specificity in the binding domain of the human androgen receptor. Implications for pathogenic gene mutations. J. Biol. Chem. *275*, 26164–26171.

687 Moras, D., and Gronemeyer, H. (1998). The nuclear receptor ligand-binding domain:
688 structure and function. Curr. Opin. Cell Biol. *10*, 384–391.

689

690 Nettles, K.W., Bruning, J.B., Gil, G., O'Neill, E.E., Nowak, J., Guo, Y., Kim, Y.,
691 DeSombre, E.R., Dilis, R., Hanson, R.N., et al. (2007). Structural plasticity in the
692 oestrogen receptor ligand-binding domain. EMBO Rep. *8*, 563–568.

693

694 Ortlund, E.A., Bridgham, J.T., Redinbo, M.R., and Thornton, J.W. (2007). Crystal
695 structure of an ancient protein: evolution by conformational epistasis. Science *317*,
696 1544–1548.

697

698 Osz, J., Brélivet, Y., Peluso-Iltis, C., Cura, V., Eiler, S., Ruff, M., Bourguet, W.,
699 Rochel, N., and Moras, D. (2012). Structural basis for a molecular allosteric control
700 mechanism of cofactor binding to nuclear receptors. Proc. Natl. Acad. Sci. USA. *109*,
701 E588–E594.

702

703 Perrière, G., and Gouy, M. (1996). WWW-Query: An on-line retrieval system for
704 biological sequence banks. Biochimie *78*, 364–369.

705

706 Pfaff, S.J., and Fletterick, R.J. (2010). Hormone binding and co-regulator binding to
707 the glucocorticoid receptor are allosterically coupled. J. Biol. Chem. *285*, 15256–
708 15267.

Ricketson, D., Hostick, U., Fang, L., Yamamoto, K.R., and Darimont, B.D. (2007). A conformational switch in the ligand-binding domain regulates the dependence of the glucocorticoid receptor on Hsp90. Mol. Biol. *368*, 729–741.

Rupprecht, R., Reul, J.M.H.M., van Steensel, B., Spengler, D., Söder, M., Berning, B., Holsboer, F., and Damm, K. (1993). Pharmacological and functional characterization of human mineralocorticoid and glucocorticoid receptor ligands. Eur. J. Pharmacol. *247*, 145–154.

Schrödinger Release 2013-1: MacroModel, version 10.0; Schrödinger, LLC: New York, NY, 2013.

Shan, Y., Gnanasambandan, K., Ungureanu, D., Kim, E.T., Hammarén, H., Yamashita, K., Silvennoinen, O., Shaw, D.E., and Hubbard, S.R. (2014). Molecular basis for pseudokinase-dependent autoinhibition of JAK2 tyrosine kinase. Nat. Struct. Mol. *21*, 579–584.

Shelley, M., Bennett, C., Nathan, D., and Sartor, O. (2008). Non-Steroidal anti-androgen use as part of combined androgen blockade therapy for metastatic or locally advanced prostate cancer: A review of the evidence on efficacy and toxicity. In

730 Cancer Metastasis-Biology and Treatment, Ablin, R.J., and Mason, M.D. ed.
731 (Springer Science and Business Media B.V.) pp. 283-307.

732

733 Shibata, S., Rinehart, J., Zhang, J., Moeckel, G., Castañeda-Bueno, M., Stiegler,
734 A.L., Boggon, T.J., Gamba, G., and Lifton, R.P. (2013). Mineralocorticoid receptor
735 phosphorylation regulates ligand binding and renal response to volume depletion and
736 hyperkalemia. Cell Metab. *18*, 660–671.

737

738 Sitruk-Ware, R., and Nath, A. (2010). The use of newer progestins for contraception.
739 Contraception *82*, 410–417.

740

741 Soisson, S.M., Parthasarathy, G., Adams, A.D., Sahoo, S., Sitlani, A., Sparrow, C.,
742 Cui, J., and Becker, J.W. (2008). Identification of a potent synthetic FXR agonist with
743 an unexpected mode of binding and activation. Proc. Natl. Acad. Sci. USA *105*,
744 5337–5342.

745

746 Sonoda, M.T., Martínez, L., Webb, P., Skaf, M.S., and Polikarpov, I. (2008). Ligand
747 dissociation from estrogen receptor is mediated by receptor dimerization: evidence
748 from molecular dynamics simulations. Mol. Endocrinol. *22*, 1565–1578.

749

Takahashi, R., Gil, V.A., and Guallar, V. (2014). Monte Carlo free ligand diffusion with markov state model analysis and absolute binding free energy calculations. J. Chem. Theory Comput. *10*, 282–288.

Waterhouse, R.M., Tegenfeldt, F., Li, J., Zdobnov, E.M., and Kriventseva, E.V. (2013). OrthoDB: A hierarchical catalog of animal, fungal and bacterial orthologs. Nucleic Acids Res. *41* (Database issue), D358–D365.

Williams, S.P., and Sigler, P.B. (1998). Atomic structure of progesterone complexed with its receptor. Nature *393*, 392–396.

Yen, P.M. (2001). Physiological and molecular basis of thyroid hormone action. Physiol. Rev. *81*, 1097–1142.

Figure 1.

Evolutionary relationship of the steroid receptors with structural comparison of GR and MR LBD

(**A**) Evolutionary relationship of the steroid hormone receptors (ERα, ERβ, MR, GR, PR and AR; decimal numbers = distance; integers = bootstrap value).

(**B**) GR (yellow) in complex with dexamethasone (magenta) overlaid on MR (lightblue) in complex with dexamethasone (magenta). The AF-2 surface is located where helices 3,4 and 12 meet.

(**C**) Details near the region where helices 3, 7 and 11 meet.

(**D**) The chemical structures of dexamethasone and dibC. The steroidal A, B, C and D rings and positions 3 and 17 are marked on the dexamethasone structure.

Figure 2.

Comparison of the complex structures of the MR:Dexa and MR:dibC

(A) Stereo view of the 2mFo-dFc density map of the MR:Dexa ligand binding pocket.

(B) The structure of MR (light blue) in complex with dexamethasone (magenta) superimposed on MR (dark blue) in complex with dibC (white). The steroid template overlays nearly perfectly (RMSD 0.28 Å) with all hydrophilic interactions conserved.

Figure 3.

Comparison of the complex structures of MR:Dexa, MR:dibC, GR:Dexa and GR:dibC

(**A**) MR (light blue) in complex with dexamethasone (magenta) overlaid on MR (dark blue) in complex with dibC (white).

(**B**) The cyclohexyl motif of dibC come into direct conflict with residues from H7 (MR:Dexa), enforcing a new structural state.

(**C**) MR (dark blue) in complex with dibC (white) superimposed on GR (yellow) in complex with dexamethasone (magenta).

(**D**) GR (yellow) in complex with dexamethasone (magenta) overlaid on GR (orange) in complex with dibC (white).

Figure 4.

Ligand exit pathway for the MR:Dexa complex

(**A**) The ligand center of mass is highlighted in blue beads. The ligand atoms are shown in transparent spacefill.

(**B**) Detail of the backbone rearrangement along the exit pathway. The MR:Dexa and MR:dibC X-ray structures are shown in light and dark blue, respectively, with dexamethasone in the binding pocket in magenta. Three protein cartoon snapshots and one pose of dexamethasone as it pass through the receptor surface from the exit simulations are shown in green.

(**C**) $\mathbf{C_\alpha}$ RMSF relative the average structure along the MR:Dexa exit pathway plotted for each residue. The dotted line denotes the average RMSF across the LBD. Helices 6 and 7 are marked with green shade.

Figure 5.

Ligand exit pathway for the GR:Dexa complex.

(A) The ligand center of mass is highlighted in blue beads. The ligand atoms are shown in transparent spacefill. **(B)** Detail of the backbone rearrangement along the exit pathway. The GR:Dexa and GR:dibC X-ray structures are shown in light yellow and orange, respectively. Three snapshots from the exit simulations are shown in green and dexamethasone in the binding pocket is shown for reference in magenta. **(C)** C_α RMSF relative the average structure along the GR:Dexa exit pathway where helices 6 and 7 are marked with green shade.

Figure 6.

Unbiased simulation of dexamethasone entering the MR binding pocket

(**A**) Each line represents the ligand heavy atom RMSD to the ligand from the crystallographic structure for a single trajectory. Two of the trajectories represented by blue and red lines enter the ligand binding pocket at step 52 and 214, respectively.

(**B**) The ligand center of mass for the two trajectories that enter the binding pocket are shown as blue and red spheres. The region where the ligands enter the binding pocket is emphasized as a surface with two ligands from the simulations shown in full stick representation.

Figure 7.

Refined ligand binding simulations and estimated binding free energy

(**A**) The protein-ligand interaction energy plotted against the ligand heavy atom RMSD to the crystallographic structure along the 400 refinement trajectories in MR:Dexa.

(**B**) MR (blue) in complex with dexamethasone (magenta) overlaid on the lowest interaction energy structure after the refined exploration (green).

(**C**) X-Z 2D projection of the PMF obtained in the MSM analysis for the same process.

Figure 8

Evolutionary conservation of the LBD for the steroid receptors

The graphs show normalized amino acid variability score for pairwise comparisons of MR (**A**), PR (**B**), AR (**C**), ERα (**D**) and ERβ (**E**) in blue vs GR in red plotted against the GR amino acid sequence. The variability score was average normalized and smoothed using a 5 amino acid sliding window. Helices 1-12 are annotated using vertical bars (green: H6-7; blue: H10-11; gray: all others). High variability scores indicate less conservation.

Table 1. Data collection and refinement statistics.

	MR: Dexa	MR: dibC	GR:dexa	GR:dibC
Data collection[a]				
PDB ID	4uda	4udb	4udc	4udd
Space group	P212121	P41212	P3221	P3221

a, *b*, *c* (Å)	73.00, 81.40, 45.23	75.92, 75.92, 117.00	84.66, 84.66, 105.91	87.20, 87.20, 102.89
α, β, γ (°)	90.00, 90.00, 90.00	90.00, 90.00, 90.00	90.00, 90.00, 120.00	90.00, 90.00, 120.00
Resolution (Å)	40.7-2.03 (2.17-2.03)	48.79-2.36 (2.55-2.36)	31.81-2.50 (2.67-2.50)	40.14-1.80 (1.85-1.80)
R_{sym} (R_{merge})	0.06(0.50)	0.13(1.30)	0.08(0.55)	0.08(1.05)
$I / \sigma I$	13.10(2.30)	15.10(1.90)	8.80(1.60)	7.40(0.70)
Completeness (%)	83.9(83.7)	100.0(100.0)	99.6(99.5)	99.9(100.0)
Redundancy	3.3(2.5)	12.6(11.7)	4.1(4.2)	3.5(3.6)
Refinement				
Resolution (Å)	2.03	2.36	2.50	1.80
No. reflections	15085	14672	15559	42339
R_{work} / R_{free}	0.185/0.240	0.182/0.218	0.210/0.253	0.213/0.224
No. atoms				
Protein	2080	2118	2133	2184
Ligand/ion	34	49	64	146
Water	101	60	83	250
B-factors				
Protein	30.14	53.25	49.72	33.25
Ligand/ion	22.12	44.16	34.51	23.55
Water	36.03	56.86	46.23	46.95
R.m.s. deviations				
Bond lengths (Å)	0.010	0.010	0.010	0.010
Bond angles (°)	1.01	1.04	1.12	1.06
Molprobity score				
Clashscore	2	1	1	1
Ramachandran outliers (%)	0	0	0.4	0
Sidechain outliers (%)	1.7	1.7	2.5	0.8

857 [a]Values in parentheses are for highest-resolution shell.

858 **Table 2**. Measurement of koff using SPR and SMM.

Ligand (method)	**GR**	**MR**
Dexa (SPR, 10 ºC)	**0.0034 s^{-1}**	**0.0011 s^{-1}**
dibC (SPR, 10 ºC)	**0.0010 s^{-1}**	**<0.0001 s^{-1}**
Dexa (SMM, 20 ºC)	**0.0070 s^{-1}**	**0.0025 s^{-1}**
dibC (SMM, 20 ºC)	**0.0029 s^{-1}**	**0.0012 s^{-1}**

859

860

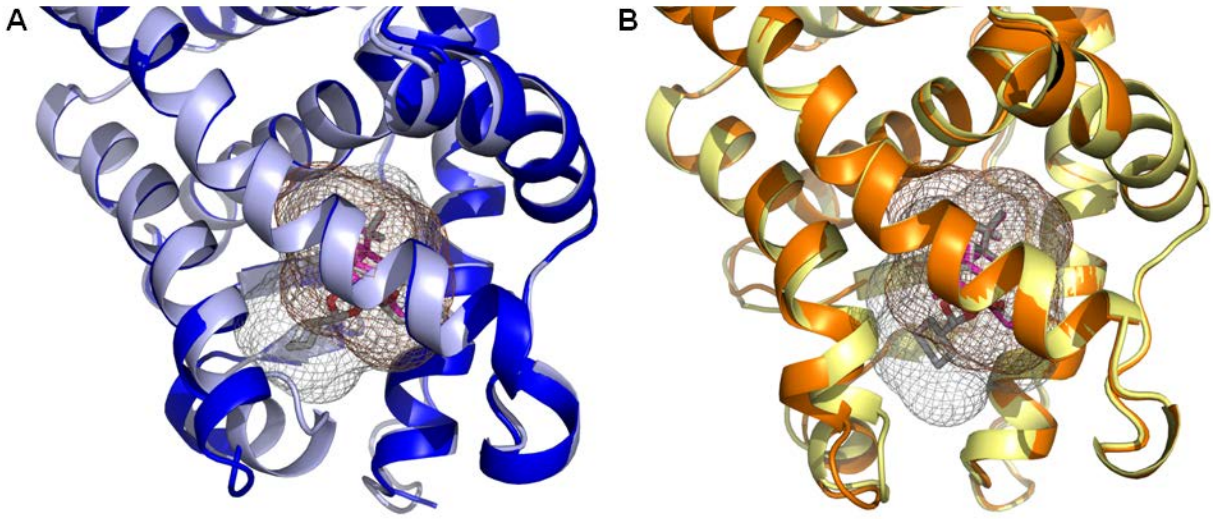

Figure S1, Related to Figure 3. Comparison of the volume of the ligand binding pocket in MR and GR in complex to Dexa and dibC. (**A**) The structure of MR (light blue) in complex with dexamethasone (magenta) overlaid on MR (dark blue) in complex with dibC (white). Ligand binding pockets are shown for MR:Dexa in brown (total volume 543 $Å^3$) and MR:dibC in gray (total volume 714 $Å^3$). (**B)** The structure of GR (pale yellow) in complex with dexamethasone (magenta) overlaid on the GR structure (orange) in complex with dibC (white). Ligand binding pockets are shown for GR:Dexa in brown (total volume 572 $Å^3$) and GR:dibC in gray (total volume 661 $Å^3$).

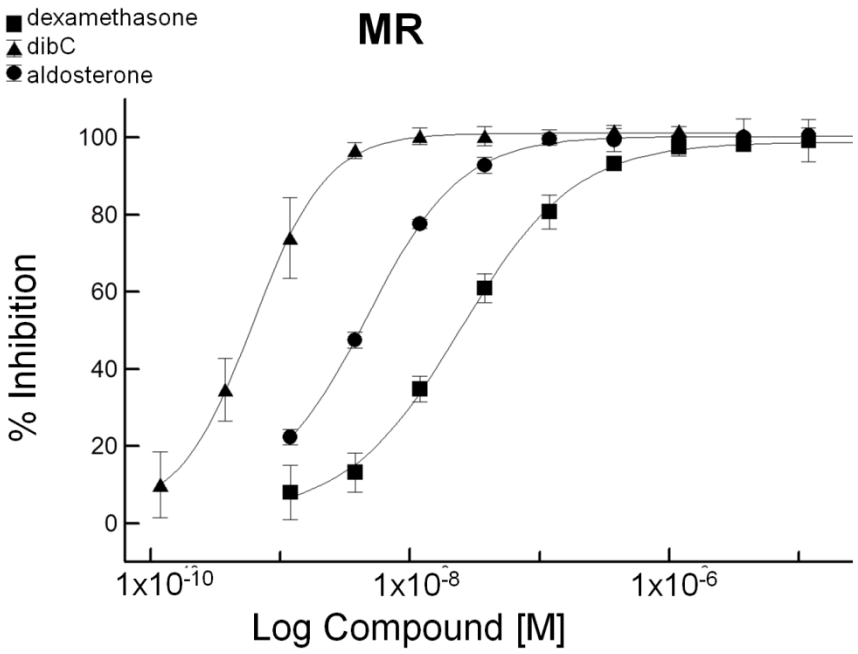

Figure S2, Related to Figure 7C. MR binding competition assay in the presence of dibC (triangle), aldosterone (circle), and dexamethasone (square). The corresponding IC_{50} values (mean ± SD, n=3) are: 0.7 ± 0.0 nM (dibC); 4.0 ± 0.2 nM (aldosterone); 26.0 ± 4.6 nM (dexamethasone).

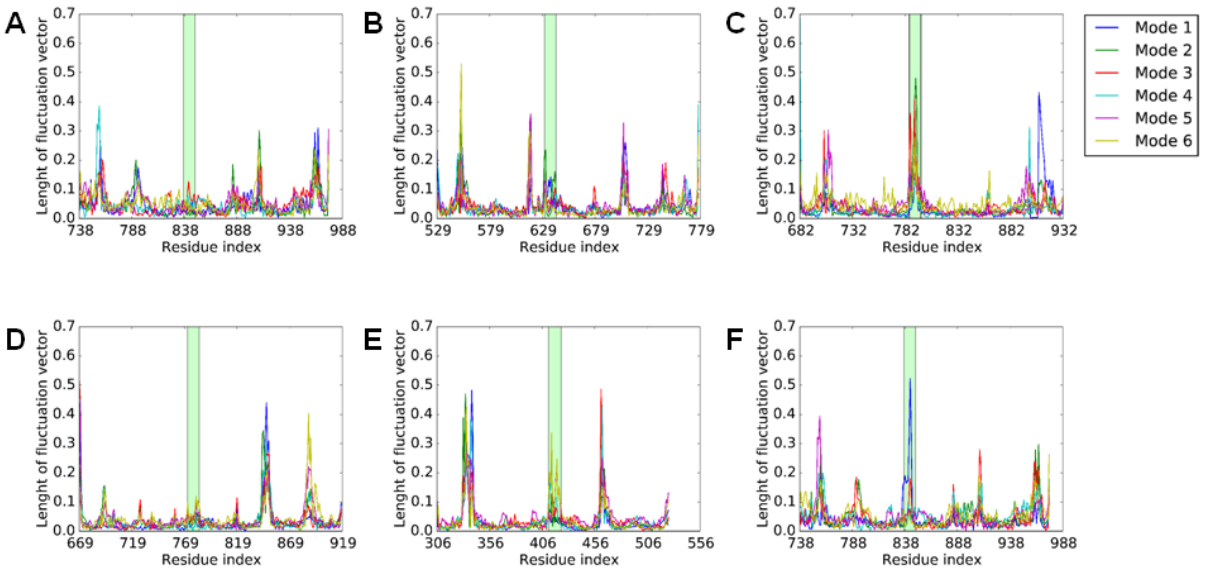

Figure S3, Related to Figure 3. Principal component analysis (PCA) for all X-ray structures of the steroid hormone receptors in the protein databank (PDB). The graphs show the amplitude of the top six modes from the PCA for MR **(A)**, GR **(B)**, PR **(C)**, AR **(D)** and ER **(E)**. The H6-H7 region which undergo the largest changes in the MR:dibC structure and the corresponding region in the other receptors are highlighted in green (MR: 837-848; GR: 631-642; PR: 786-797; AR: 772-783; and ER: 412-424). AR and MR exhibits the smallest variation in the H6-H7 region in the public domain structures. **(F)** The PCA of the MR public domain structures with MR:dibC added. In this analysis the mode describing the H6-H7 rearrangement becomes the dominant signal in the first mode.

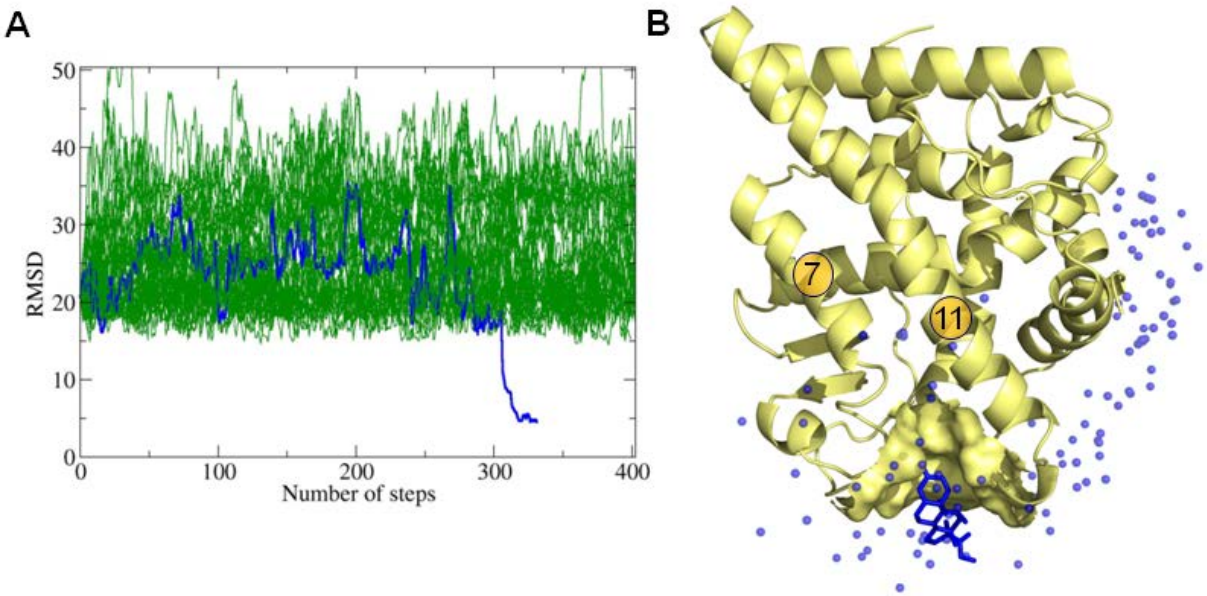

Figure S4, Related to Figure 6. Unbiased simulation of dexamethasone entering GR. **(A)** Each line represents the ligand heavy atom RMSD to the crystallographic structure for the total 64 trajectories. One of the trajectories represented by blue line enter the ligand binding pocket at step ~310. **(B)** The ligand's center of mass for the one trajectory that enter the binding pocket are shown as blue spheres. The region where the ligand enter the binding pocket is emphasized as a surface with the ligand shown in stick representation.

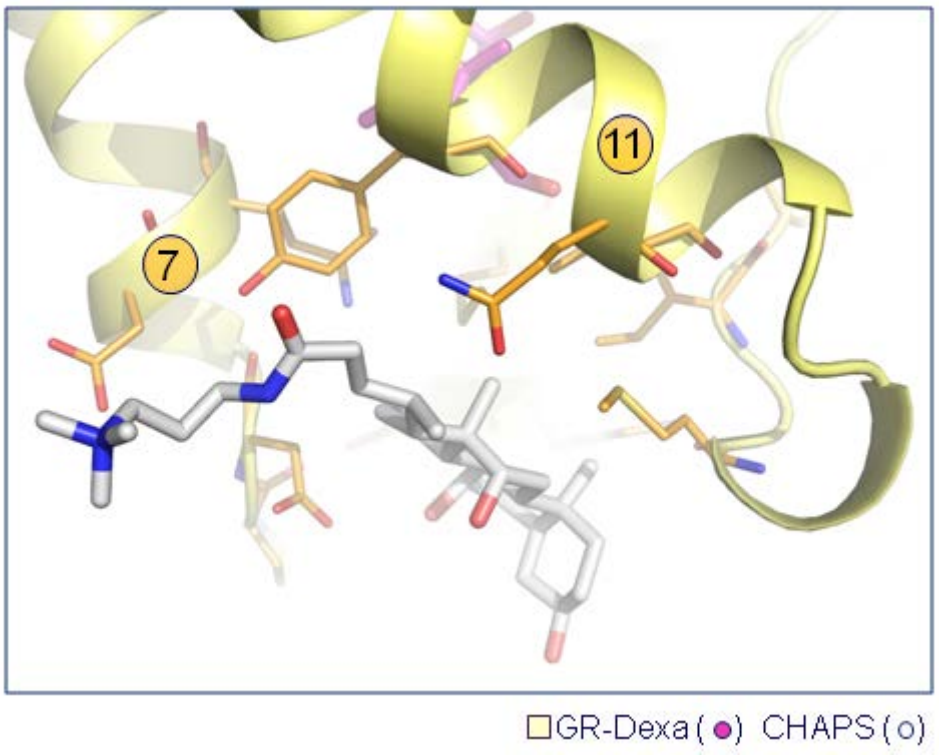

Figure S5, Related to Figure 3. The peripheral binding site. The structure of of GR (yellow) in complex with dexamthasone (magenta) revealed that a CHAPS molecule (white) from the protein formulation is binding in between helices 7 and 11 about 12 Å away from the ligand binding pocket.

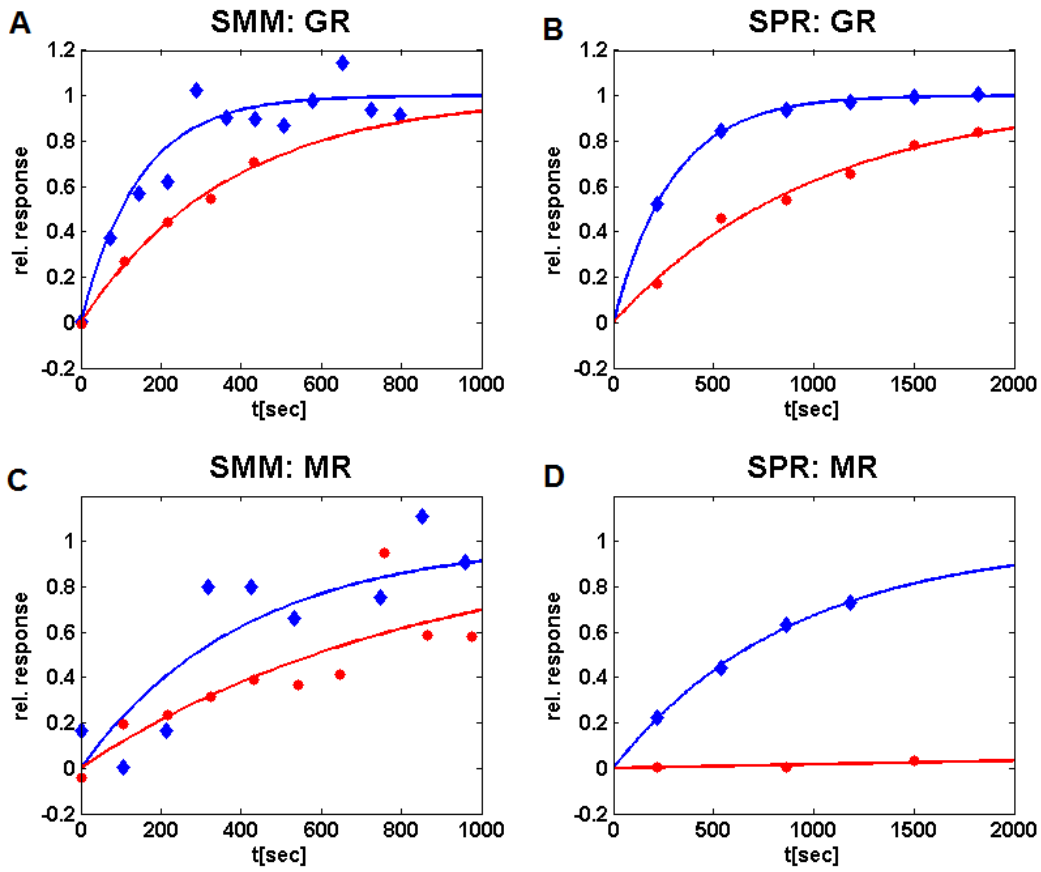

Figure S6, Related to Table 2. Residence time measurements of dexamethasone (blue diamonds) and dibC (red circles) bound to GR **(A, B)** and MR **(C, D)** using SMM **(A, C)** and SPR **(B, D).** Normalized change in receptor binding rate to surface-immobilized co-regulator peptide upon addition of >10-fold concentration excess of budesonide (GR) or aldosterone (MR). The extracted binding rates are fitted with $k_+(t) = ae^{-k_{off}t} + c$ (colored solid lines). SMM and SPR experiments were conducted 20 °C and 10 °C, respectively.

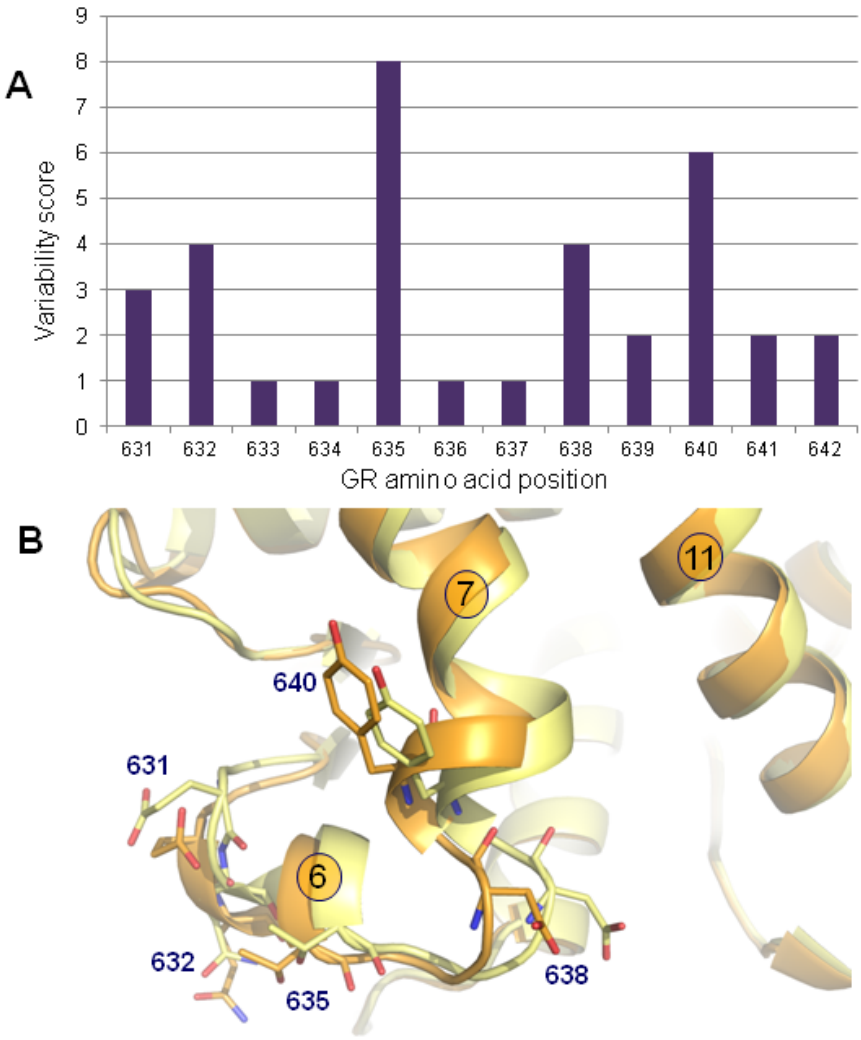

927

928 **Figure S7, Related to Figure 8**. Variability score and structural arrangement of
929 amino acids in the H6-H7 region in GR. (A) The GR variability scores plotted against
930 the amino acid positions of the H6-H7 region. Higher scores indicate more variation
931 at that position across the various species; a score of 1 indicate completely
932 conservation. (B) Placement of amino acids with high variability score in the H6-H7
933 region in the GR:Dexa (yellow) and GR:dibC (orange) structures.

Supplementary Movie, Related to Figure 4. Unbiased simulation of dexamethasone entry into MR obtained with the PELE (Protein Energy Landscape Exploration) software. The simulated protein is shown in green, the NCOA1 peptide cofactor in yellow and dexamethasone ligand shown in light green. At the 0:27 timepoint, the MR:Dexa complex structure is overlaid onto the simulation for comparison with the protein in light blue and dexamethasone in magenta.

Supplemental experimental procedures

Protein expression and purification for structure

GR:Dexa

The cDNA sequence encoding the human GR-LBD (amino acids 500-777) with the mutations N517D, F602S and C638D and an N-terminal 6-histidine tag followed by a thrombin cleavage site was cloned into a pFastBac-HTb vector (Life Technologies). Recombinant baculovirus was generated using the Bac-to-Bac expression system (Life Technologies) and High Five cells (Life Technologies) were infected followed by suspension culture in Express Five medium (Gibco) for 48h at 27°C, the last 24h in the presence of 10 μM dexamethasone, after which cells were collected by centrifugation. All protein purification steps were performed at 4°C. Cells were lysed in buffer A (50 mM Tris pH 8.0, 2.5 mM DTT, 1% CHAPS, 50 μM dexamethasone and 10% glycerol) supplemented with Complete EDTA-free protease inhibitor cocktail (Roche) followed by affinity purification using Ni-NTA beads (Qiagen). Protein was eluted in buffer A supplemented with 150 mM NaCl and 300 mM imidazole, and subjected to size exclusion chromatography using a HiLoad 26/60 Superdex 200 gel filtration column equilibrated in buffer A. Five-fold molar excess of a TIF2 peptide, KENALLRYLLDK (Innovagen) was added, the N-terminal 6-histidine tag was removed using thrombin-agarose (Sigma) and subsequently the free 6-histidine tag was removed. The protein was thereafter passed over a Q Sepharose fast-flow ion-exchange column (GE Healthcare) equilibrated in buffer A and stored at −80 °C. Approximately 5.4 mg protein was obtained from 10 L High Five cells.

GR:dibC

A pFastBac (Invitrogen) construct encoding human GR-LBD (amino acids 500-777) with the mutations N517D, V571M, F602S and C638D and an N-terminal, thrombin cleavable 6-His tag was used to generate baculoviruses in Sf9 cells (Invitrogen). GR-LBD encoding viruses were used to infect High Five cells (Invitrogen) at a density of 2-3x10E6 cells/ml and a MOI of 3 in a Wave Bioreactor at 27^{o}C. 24 hours post-infection, dexamethasone was added to a final concentration of 10 µM. The cells were harvested by centrifugation 48 hours post-infection, washed in PBS and stored at -80°C until lysis. Cells were resuspended in lysis buffer (50 mM Tris-HCl pH 8.0, 10% glycerol, 1% CHAPS, 2.5 mM DTT, Complete EDTA-free protease inhibitor cocktail (Roche) and 50 µM dexamethasone) and lysed by 5x1 min passes in a polytron homogeniser. The cell-lysate was clarified by centrifugation at 18500 g for 90 minutes and batch-bound to Ni-NTA Superflow (Qiagen) for 1.5 hours at 4°C. The IMAC resin was packed in a column, washed with wash buffer (50 mM Tris pH8.0, 60 mM NaCl, 30 mM imidazole, 10% glycerol, 1% CHAPS, 2.5 mM DTT and 50 µM dexamethasone) and GR-LBD was step eluted with elution buffer (50 mM Tris pH 8.0, 30 mM NaCl, 300 mM imidazole, 10% glycerol, 1% CHAPS, 2.5 mM DTT and 50 µM dexamethasone). The eluate was loaded on a HiLoad 26/60 Superdex 200 size exclusion column equilibrated in gel filtration buffer (50 mM Tris-HCl pH 8.0, 10% glycerol, 1% CHAPS, 2.5 mM DTT and 50 µM dexamethasone). GR containing fractions were pooled and a 3-fold excess of co-activator NR-box peptide (KENALLRYLLDK, human NCoA2, residues 740-751) was added. The His-tag was cleaved over night at 4^{o} C with Thrombin-agarose (Sigma) and removed by negative IMAC using Ni-NTA. The protein was finally polished through Q Sepharose FF (GE

Healthcare) equilibrated in gel filtration buffer, flash-frozen in liquid nitrogen and stored at -80^{o}C.

MR:Dexa and MR:dibC

Human MR-LBD (amino acids 735-984) with the mutations C808S, C910S (and S810L in the case of dibC), an N-terminal, TEV cleavable 6-HN tag, and a C-terminal thrombin cleavable co-activator peptide PQAQQKSLLQQLLTE was cloned into pET24a(+). *Escherichia coli* BL21 StarTM (DE3) (Invitrogen) cells transfomed with the expression vector were grown in terrific broth at 37°C until OD600=0.5-1.0, chilled on ice for 30 minutes and 100 µM of dexamethasone (Alfa Aesar) or dibC was added. Cells were shaken at 16°C for 30 minutes before protein production was induced using 0.1 mM isopropyl β-D-thiogalactopyranoside (IPTG) for an additional 24-48 hours. Cells were lysed in 30 mM Na-Hepes pH 7.5, 150 mM NaCl, 20 mM imidazole, 100 mM arginine-HCl, 10% glycerol, 1% CHAPS and 1 mM TCEP containing 20 µM of respective ligand, EDTA-free Complete protease inhibitor cocktail (Roche) and 0.05 g/ml of CelLytic™ Express (C1990, SIGMA), by rotation at room-temperature for 15 minutes. The lysate was cleared by centrifugation at 48000 g for 20 minutes and loaded onto Ni-Sepharose FF (GE Healthcare) equilibrated in lysis buffer. After washing, protein was step eluted by the addition of one column volume (CV) of lysis buffer containing 0.5 M Arginine-HCl followed by 5 CV of elution buffer (30 mM Na-Hepes, pH 7.5, 150 mM NaCl, 500 mM imidazole, 500 mM arginine-HCl, 10% glycerol, 1% CHAPS, 1 mM TCEP and 20 µM of respective ligand). Size exclusion chromatography was performed on a HiLoad Superdex 200 column (GE Healthcare) equilibrated in 20 mM Na-Hepes pH 6.7, 150 mM NaCl, 0.5 M arginine-HCl, 10% glycerol, 0.1% CHAPS, 1 mM TCEP and 2 µM dexamethasone or dibC. Finally, MR-LBD co-expressed with dexamethasone was diluted 10x in 20

mM Tris-HCl pH 8.0, 10 mM $CaCl_2$ and 20 µM dexamethasone, cleaved with TEV protease and Thrombin CleanCleave Kit (SIGMA), purified by reverse IMAC on Ni-Sepharose FF and concentrated to 15 mg/ml. MR-LBD co-expressed with dibC was diluted 15x in 10 mM Tris-HCl pH 8.5, 20 µM dibC and 1mM TCEP and concentrated to 7 mg/ml.

Protein expression and purification for biophysical characterization

GR

Human GR-LBD (amino acids 529-777) was cloned into the pET24a vector (Novagen) featuring an N-terminal His_6-tag and a TEV protease cleavage site. The expression vector was transformed into E. coli BL21(DE3) STAR, followed by expression in PASM-5052 autoinduction medium. 100 µM dexamethasone was added after the cell culture reached an OD of 0.6 followed by expression over 48 hours at 16 °C. All purification buffers were degassed and contained 2 mM TCEP and 50 µM dexamethasone. The harvested cells were resuspended in lysis buffer (50 mM Tris pH 8, 10% glycerol, 1% CHAPS) supplemented by protease inhibitors (Complete, Roche) and DNAse. Cells were lysed by sonication. The cleared lysate was applied to a nickel affinity column equilibrated with wash buffer (50 mM Tris pH 8, 10% glycerol, 1% CHAPS, 60 mM NaCl) and eluted by a 300 mM imidazole gradient. Remaining impurities were removed by an additional superdex 200 gelfiltration step using 50 mM Tris buffer at pH 9 as running buffer followed by storage at -80°C.

MR

Human MR-LBD (amino acids 712-984) with the mutation C808S and an N-terminal, TEV cleavable 6-HN tag was cloned and expressed in the same way as the MR–LBD proteins used for structure determination. The cells were lysed in 50 mM Tris-

HCl, pH 8.0, 500 mM NaCl, 100 mM arginine-HCl, 1% CHAPS, 20 mM imidazole, 10% glycerol, 1mM TCEP, 50 µM dexamethasone, EDTA-free Complete protease inhibitor cocktail (Roche) and 0.05 g/ml of CelLytic™ Express (C1990, SIGMA). The lysate was cleared by centrifugation at 48000 g for 20 minutes and loaded onto a HisTrap HP column (GE Healthcare). The protein was gradient eluted with 50 mM Tris-HCl, pH 8.0, 500 mM NaCl, 500 mM arginine-HCl, 1% CHAPS, 0- 300 mM imidazole, 10% glycerol, 1mM TCEP, 50 µM dexamethasone.

Crystallization

GR:Dexa

A tube with 1.0 mg of GR(500-777) N517D, F602S and C638D was thawed and washed three times in the concentrator tube with 3.5 ml of 10 mM Tris pH 8.5, 2.5 mM DTT and 45µM dexamethasone. A fivefold molar excess of co-activator NR-box peptide (KENALLRYLLDKDD, human NCoA2, residues 740-753) was added and the complex was concentrated to 9 mg/ml.

Crystals were grown at 4°C in hanging drops using 1 µl of protein and 1 µl of well solution (10% PEG8000, 10% ethylene glycol and 0.1 M Hepes pH 7.5). Crystals were frozen in liquid nitrogen with 20% ethylene glycol as cryo protectant prior to data collection.

GR:dibC

A tube with 5.0 mg's of GR(500-777) N517D, V571M, F602S and C638D was thawed and concentrated to about 1.5 ml. The protein was washed three times in the concentrator tube with 10 ml of 10 mM Tris pH 8.5, and 2.5 mM DTT (buffer B) to remove excess of dexamethasone and thereafter diluted to a final volume of 6 ml. dibC was added to a final concentration of 0.25 mM to boost ligand exchange prior to

dialysis. Dialysis was performed using two Slide-A-Lyzer dialysis cassettes in a beaker containing buffer B and 60 µM of dibC. Dialysis solution was exchanged after 20, 28 and 46 hours before harvesting the sample. The protein was concentrated to 1 ml and buffer was exchanged to fresh buffer B using a NAP10 column. A twofold molar excess of co-activator NR-box peptide (KENALLRYLLDKDD, human NCoA2, residues 740-753) was added and the complex was concentrated to 9 mg/ml.

Crystals were grown at 4°C in hanging drops using 2 µl of protein and 1 µl of well solution (10% PEG8000, 20% ethylene glycol and 0.1 M Hepes pH 7.5). Crystals appeared as rod like crystals after 1-2 days but continued to grow for one to two weeks. Crystals were frozen in liquid nitrogen without any cryo protectant prior to data collection.

MR:Dexa

Crystals of MR(735-984) C808S and C910S co-expressed and purified with dexamethasone were grown by sitting drop vapor diffusion in 30% PEG4000, 0.1 M NaCl and 0.2 M Pipes pH 7.4. Crystals were cryo-protected in well solution supplemented with 20% glycerol and flash frozen in liquid nitrogen.

MR:dibC

Crystals of MR(735-984) C808S, C910S and S810L co-expressed and purified with dibC were grown by sitting drop vapor diffusion in 18% PEG4000, 0.14 M LiSO4, 85 mM Tris pH 8.5 and 15% glycerol. Crystals were flash frozen in liquid nitrogen.

Data collection and structure determination.

The MR:Dexa data were collected using an Rigaku FRE rotating anode (wavelength 1.54 Å). The GR:Dexa data were collected at the ID14:4 beam line at the ESRF

(wavelength 0.94 Å). The MR:dibC and GR:dibC data were collected at the ID29 beam line et the ESRF (wavelength 0.98 Å). All data sets were collected from a single crystal at 100K. The MR data sets were integrated with XDS (Kabsch et al., 2010) and the GR data sets were integrated with Mosflm (Leslie et al., 2007). All data sets were merged with SCALA (Evans et al., 2006) from the CCP4 suite (Collaborative Computational Project., 1994). The MR and GR structures were solved with PHASER (McCoy et al., 2007) using PDB entry 2AA2 and 1M2Z as starting models, respectively. The structures were refined using the BUSTER (Bricogne et al., 2011) and manual rebuilding using Coot (Emsley et al., 2004). The GR:Dexa structure had 1 (0.39%) Ramachandran outlier while the other structures did not have any outliers. All figures were prepared using PyMOL (*www.pymol.org*).

Structural analysis

Cavity volumes were calculated with fpocket 2.0 (Le Guilloux et al. 2009). For a higher accuracy, the default number of Monte Carlo steps was increased from 2500 to 500000. The minimum size of alpha spheres was set to 3.5 Å to avoid connecting buried cavities (default value 3.0 Å).

PCA analysis was performed using ProDy 1.5.1 (Bakan et al. 2011) For each receptor, all public available structures were included in the analysis and one structures was selected as the reference structure (MR:Dexa, GR:Dexa, 1E3G (AR), 1A28 (PR), 1A52 (ER)). The sequence of monomer A from each protein was aligned to the sequence of the reference structure filtering out structures with less than 90% sequence identity and subsequently superimposed. The first six principal

components were plotted against the residue number by calculating the length of the x,y,z-fluctuation vector for each c-alpha atom.

Mineralocorticoid receptor ligand competition binding assay

Human MR-LBD (729-984) with an N-terminal maltose binding protein (MBP) tag was expressed using the Bac-to-Bac expression system (Life Technologies). High Five cells were co-infected with recombinant P23 co-chaperone baculovirus followed by suspension culture in Express Five medium (Gibco) for 48h at 27°C. Cells were lysed in lysis buffer (10 mM Tris-HCl pH 7.4, 0.5 mM EDTA, 2.5 mM DTT, 10% glycerol, 20 mM Na_2MoO_4 and Complete protease inhibitor (Roche)) followed by centrifugation. The supernatant was stored at -80°C. Compound binding was assessed using a ligand competition binding scintillation proximity assay (SPA). Compounds were incubated with MR-High Five cell lysate (7μg/ml) and 5 nM ^{3}H-aldosterone (Perkin Elmer NET419250UC) in assay buffer (10 mM Tris-HCl, 0.5 mM EDTA, 20 mM Sodium molybdate dehydrate, 10 % Glycerol and 0.1 mM DTT) for one hour before addition of 2.5 mg/ml anti-rabbit SPA PS beads (Perkin Elmer RPNQ0299) and 2 µg/ml rabbit anti-MBP antibodies (Abcam ab9084) followed by incubation at room temperature for 8 hours before detection of signal using a LeadSeeker imaging system (GE Healthcare). Ki values where derived using the equation Ki = (IC50 - receptor Concentration/2) / (1 + ligand Conc/Km), where receptor concentration was set to zero, ligand concentration to 0.005 µM and Km-value to 0.0016 µM.

Biophysical characterization and residence time determination

Residence time measurements of GR/MR:dexamethasone and dibC was determined using single molecule microscopy (SMM) and SPR (Biacore) by probing the time-reolved change in receptor binding to surface-immobilized co-regulator peptides (GR: Biotin-PRGC1_130-155 / MR: PRGC2_146-166). HBSP(+) buffer (10 mM HEPES, 150 mM NaCl, 0,005% P20, pH=7.4) was used for all measurements. For SPR, the two biotinylated peptides was immobilized on a strepavidin chip (GE healthcare) using a Biacore 3000 (GE healthcare) to 500-1000 RU. Budesonide/aldosterone was added to a final concentration of 25 µM to a solution of 130 nM GR/MR, preequilibrated with 1µM dexamethasone/dibC. Directly after budesonide/aldosterone addition, receptor binding rate to the cofactor peptide was monitored by consecutive injection cycles (1 min injections). The peptide surface was regenerated with 0.005% SDS after each injection. To compensate for potential protein degradation over the time course of the measurement, the data was normalized to a reference sample containing only 1uM dexamethasone/dibC. For SMM, the respective NHR was bound via 6×His-tag to liposomes containing POPC, DGS-NTA, lissamine rhodamine B sulfonyl in a ratio of 1:0.02:0.01. Liposomes were prepared as described by Gunnarsson Anal chem. 2015. The coregulator peptides were mixed with Neutravidin (NA) in a 1:1 molar ratio. Subsequently, the coregulator peptide-NA complex was incubated at 50 µg/ml NA with TL1 cleaned PLL-*g*-PEG/ PLL-*g*-PEG-biotin (1:1, Surface Solutions) coated glass surfaces. Budesonide/aldosterone was added to a final concentration of 10 µM to a 150 pM liposome-NHR solution containing 1 µM dexamethasone/dibC. To compensate for potential protein degradation over time the data was normalized to a reference sample of 150 pM liposome-NHR solution containing only 1uM dexamethasone/dibC. Image data was collected on an inverted

microscope (Nikon Ti Eclipse) equipped with a 60x oil immersion objective (NA = 1.49), TRITC filter cube, perfect focus system and air cooled sCMOS (Orca Flash 4.0 v2 Hamamatsu). For imaging in an iterative fashion, 10 sec time series at 10Hz framerate were recorded for the competition and the reference well at two different positions continuously over ~15 minutes. Images were analyzed using custom made Matlab (Mathworks) routines to extract the liposome-NHR conjugate binding rate to the surface. The liposome-NHR binding rate during each time series (10 sec) was assumed to be constant and hence, the vesicle binding rate was extracted by linear regression to the cumulative number of binding liposomes as a function of time. To compensate for surface preparation inhomogeneities the data of the two different positions in each well were averaged. The extracted binding rates were plotted over time and fitted with $k_+(t) = ae^{-k_{off}t} + c$.

Supplemental references

Bakan, A., Meireles, L.M., and Bahar, I. (2011). ProDy: protein dynamics inferred from theory and experiments. Bioinformatics *27*, 1575–1577.

Bricogne, G., Blanc, E., Brandl, M., Flensburg, C., Keller, P., Paciorek, C., Roversi, P., Sharff, A., Smart, O. S., Vonrhein, C., et al. (2011). BUSTER version 2.11.5. Cambridge, United Kingdom; Global Phasing Limited.

Collaborative Computational Project, Number 4. (1994). The CCP4 suite: programs for protein crystallography. Acta Crystallogr. D Biol. Crystallogr. *50*, 760–763.

Emsley, P., and Cowtan, K. (2004). Coot: model-building tools for molecular graphics. Acta Crystallogr. D Biol. Crystallogr. *60*, 2126–2132.

Evans, P. (2006). Scaling and assessment of data quality. Acta Crystallogr. D Biol. Crystallogr. *62*, 72–82.

Kabsch, W. (2010). XDS. Acta Crystallogr. D Biol. Crystallogr. *66*, 125–132.

Le Guilloux, V., Schmidtke, P., and Tuffery, P. (2009). Fpocket: an open source platform for ligand pocket detection. BMC Bioinform. *10*, 168.

Leslie, A.G.W., and Powell, H.R. In Evolving Methods for Macromolecular Crystallography 41–51 (Springer, Dordrecht, The Netherlands, 2007).

McCoy, A.J., Grosse-Kunstleve, R.W., Adams, P.D., Winn, M.D., Storoni, L.C., and Read, R.J. (2007). Phaser crystallographic software. J. Appl. Crystallogr. *40*, 658–674.